# Rapid 3-D magnetotelluric inversion

Gábor Hursán and Michael Zhdanov

*University of Utah, Department of Geology and Geophysics, Salt Lake City, UT 84112*

July 12, 2001

**Abstract**

A new method of rapid 3-D magnetotelluric inversion has been developed based on ideas of quasi-analytical (QA) approximation for forward magnetotelluric field modeling. We implemented several modifications of the QA method, resulting in increasing speed and resolving power of this technique. In particular, we introduced a new diagonalized form of QA approximation, which simplified the forward and inverse problem solution without loosing the accuracy. Based on the diagonalized QA approximation, we calculated the Frechet derivative (sensitivity) matrix for a magnetotelluric problem in a closed form. Also, we used an effective technique for the Green's tensor calculations based on the convolution theorem and FFT method. As a result, we constructed a rapid inversion method which could be used for 3-D inversion of the array magnetotelluric data within a few minutes on a PC. The effectiveness of the method was demonstrated on the synthetic models. We present several case histories, including interpretation of a 3-D MT survey in the southern part of Hokkaido, Japan, and inversion of 3-D MT data in the Voisey's Bay Ni-Cu-Co deposit.

# Introduction

Interpretation of array magnetotelluric (MT) data over 3-D geoelectrical structures remains one of the most challenging problems of electromagnetic geophysics. During recent years, considerable advances have been made in this area (Madden and Mackie, 1989; Eaton, 1989; Smith and Booker, 1991; Zhdanov and Keller, 1994; Newman and Alumbaugh, 1996, 1997; Alumbaugh and Newman, 1997; Zhdanov and Fang, 1996, 1999; Golubev et al., 1999; Zhdanov et al., 2000a).

Recently Zhdanov and Hursán (2000) developed a new approach to 3-D electromagnetic inversion based on the quasi-analytical (QA) approximation (Zhdanov et al., 2000b). The effectiveness of this technique was illustrated by numerical examples of controlled source EM data inversion.

Key elements of an effective inversion scheme include 1) a fast, simple and adequately accurate forward operator capable of handling large scale problems, 2) an inversion scheme for solving ill-posed problems, and 3) an effective sensitivity matrix computation algorithm, if a gradient-type inversion scheme is used.

The forward operator used in this paper bears two properties distinguishing it from that is used by Zhdanov and Hursán (2000): a) it has been extended for modeling typical magnetotelluric data, b) a diagonalized form of QA approximation is introduced, resulting in a great reduction of operation complexity without a significant loss of accuracy.

The inversion algorithm is similar to the one described in Zhdanov and Hursán (2000). It uses the Tikhonov regularization with an option of smooth and focusing geoelectric images. The minimization is performed using the reweighted regularized conjugate gradient (RRCG) method. We improved the inversion scheme by introducing the logarithm of the total conductivity as a model parameter, automatically

enforcing the positivity of the conductivity.

Since a gradient-type method is used, we specify the sensitivity (Frechet derivative) matrices for anomalous field and magnetotelluric problems as well. Additionally, we use the convolution properties of the Green's operators for economical matrix manipulations.

These modifications result in constructing a rapid numerical method of 3-D magnetotelluric inversion, which, nevertheless, provides a fine and accurate image of the underground geoelectrical structures. Synthetic MT data inversion demonstrates the resolving power of this technique.

The case histories presented here include interpretation of a 3-D magnetotelluric (MT) survey conducted by the New Energy and Industrial Technology Development Organization (NEDO) in the Minamikayabe area located in the southern part of Hokkaido, Japan, and inversion of three-dimensional magnetotelluric (MT) data collected by INCO in the Voisey's Bay Ni-Cu-Co deposit. The interpretation of real data shows that 3-D MT inversion of the huge array data can be completed on a PC within several minutes.

# Quasi-analytical approximations as forward operators for inversion

For completeness, we begin our paper with a brief review of the basic principles of QA approximation, following Zhdanov et al., (2000b) and Zhdanov and Hursán (2000).

## The method of integral equations

Consider a 3-D geoelectrical model with a background (normal) conductivity $\sigma_b$ and local inhomogeneity $D$ with the arbitrary spatial variations of conductivity $\sigma = \sigma_b + \Delta\sigma$. The backgrond conductivity is chosen to be horizontally layered half-space.

We assume that $\mu = \mu_0 = 4\pi \times 10^{-7} H/m$, where $\mu_0$ is the free-space magnetic permeability. The model is excited by an electromagnetic field generated by an arbitrary source. This field is time harmonic as $e^{-i\omega t}$, where $\omega = 2 * \pi f$ is the angular frequency. In this paper we consider the quasi-static model of the field, neglecting the displacement currents (Zhdanov and Keller, 1994).

The electromagnetic fields in this model can be presented as a sum of background (normal) and anomalous fields:

$$\mathbf{E} = \mathbf{E}^b + \mathbf{E}^a, \quad \mathbf{H} = \mathbf{H}^b + \mathbf{H}^a, \tag{1}$$

where the background field $\mathbf{E}^b$ is a field generated by the given sources in the model with background distribution of conductivity $\sigma_b$, and the anomalous field $\mathbf{E}^a$ is produced by the anomalous conductivity distribution $\Delta\sigma$.

The standard integral formulation of the electromagnetic field is the following (Hohmann, 1975; Weidelt, 1975):

$$\mathbf{E}^a(\mathbf{r}_j) = \int\int\int_D \widehat{\mathbf{G}}_E(\mathbf{r}_j \mid \mathbf{r})\, \Delta\sigma(\mathbf{r}) \left(\mathbf{E}^b(\mathbf{r}) + \mathbf{E}^a(\mathbf{r})\right) dv, \tag{2}$$

$$\mathbf{H}^a(\mathbf{r}_j) = \int\int\int_D \widehat{\mathbf{G}}_H(\mathbf{r}_j \mid \mathbf{r})\, \Delta\sigma(\mathbf{r}) \left(\mathbf{E}^b(\mathbf{r}) + \mathbf{E}^a(\mathbf{r})\right) dv, \tag{3}$$

where $\widehat{\mathbf{G}}_E(\mathbf{r}_j \mid \mathbf{r})$ and $\widehat{\mathbf{G}}_H(\mathbf{r}_j \mid \mathbf{r})$ are the electric and magnetic Green's tensors defined for an unbounded conductive medium with the background conductivity $\sigma_b$.

Expression (2) becomes a singular vector Fredholm integral equation of the second kind with respect to the anomalous electric field $\mathbf{E}^a$, if we consider the points $\mathbf{r}_j$ within the domain $D$ with anomalous conductivity. In practice, we need to solve a large system of linear equations to find the exact solution of this problem, making the full integral equation solution impractical for inversion purposes, where a rapid forward modeling scheme is needed.

## Quasi-analytical approximation for the anomalous fields

A powerful alternative to the full integral equation solution is to approximate the rigorous solution using relatively inexpensive algorithms (Born, 1933; Habashy et al., 1993; Zhdanov and Fang, 1996; Zhdanov et al., 2000b). These techniques provide not only an option for fast forward modeling, but they are useful in the construction of inversion schemes as well (Torres-Verdin and Habashy, 1994; Zhdanov and Fang, 1997; Zhdanov and Hursán, 2000).

In this paper we use the quasi-analytical (QA) approximation, where the anomalous electromagnetic field is expressed using the following integral representations (Zhdanov et al., 2000b):

$$\mathbf{E}^a(\mathbf{r}_j) \approx \mathbf{E}^a_{QA}(\mathbf{r}_j) = \int_D \widehat{\mathbf{G}}_E(\mathbf{r}_j \mid \mathbf{r}) \frac{\Delta\sigma(\mathbf{r})}{1-g(\mathbf{r})} \mathbf{E}^b(\mathbf{r})\, dv, \tag{4}$$

$$\mathbf{H}^a(\mathbf{r}_j) \approx \mathbf{H}^a_{QA}(\mathbf{r}_j) = \int_D \widehat{\mathbf{G}}_H(\mathbf{r}_j \mid \mathbf{r}) \frac{\Delta\sigma(\mathbf{r})}{1-g(\mathbf{r})} \mathbf{E}^b(\mathbf{r})\, dv. \tag{5}$$

Here function $g(\mathbf{r})$ is the normalized dot product of the Born approximation, $\mathbf{E}^B$, and the background field, $\mathbf{E}^b$ inside the anomalous domain, $D$:

$$g(\mathbf{r}) = \frac{\mathbf{E}^{B*}(\mathbf{r}) \cdot \mathbf{E}^b(\mathbf{r})}{\mathbf{E}^{b*}(\mathbf{r}) \cdot \mathbf{E}^b(\mathbf{r})}, \text{ assuming } \mathbf{E}^{b*}(\mathbf{r}) \cdot \mathbf{E}^b(\mathbf{r}) \neq 0, \tag{6}$$

where "*" means complex conjugate vector.

The Born approximation is computed by the formula

$$\mathbf{E}^B(\mathbf{r}) = \int_D \widehat{\mathbf{G}}_E(\mathbf{r} \mid \mathbf{r}') \Delta\sigma(\mathbf{r}') \mathbf{E}^b(\mathbf{r}')\, dv'. \tag{7}$$

Note that the only difference between the QA approximation and the Born approximation (7) is in the presence of the scalar function $[1-g(\mathbf{r})]^{-1}$. The computational expense of the the QA approximation is practically the same as the cost of the Born approximation inside the anomalous body. On the other hand, it is demonstrated in

Zhdanov et al. (2000b) that the accuracy of QA approximation is much higher than the accuracy of the Born approximation.

In practice we usually solve forward and inverse problems in the space of discrete data and model parameters.

Suppose that $M$ measurements of the electric or magnetic field are performed in some electromagnetic experiment. Then we can consider these values as the components of electric, $\mathbf{e}^r$ or magnetic, $\mathbf{h}^r$, vectors of a length $3M$:

$$\mathbf{e}^r = [E_x^{r1}, ..., E_x^{rM}, E_y^{r1}, ..., E_y^{rM}, E_z^{r1}, ..., E_z^{rM}]^T,$$

$$\mathbf{h}^r = [H_x^{r1}, ..., H_x^{rM}, H_y^{r1}, ..., H_y^{rM}, H_z^{r1}, ..., H_z^{rM}]^T,$$

where the superscript "$T$" denotes a transpose operation of a vector row into a vector column. Superscript "$r$" means that the field is expressed at the receiver sites.

Let us discretize the anomalous domain $D$ into $N$ cells such that the anomalous conductivity is constant within each cell. Then, the anomalous conductivity distribution $\Delta\sigma(\mathbf{r})$ can be represented as the components of a vector $\mathbf{m}$ of length $N$:

$$\mathbf{m} = [m_1, m_2, ..., m_N]^T = [\Delta\sigma_1, \Delta\sigma_2, ..., \Delta\sigma_N]^T.$$

Using these notations, we can write the discrete analogs of the quasi-analytical approximations (4) and (5), as (Zhdanov and Hursán, 2000):

$$\mathbf{e}_{QA}^{a,r} = \widehat{\mathbf{A}}_E \hat{\mathbf{B}} \mathbf{m} \tag{8}$$

and

$$\mathbf{h}_{QA}^{a,r} = \widehat{\mathbf{A}}_H \hat{\mathbf{B}} \mathbf{m}, \tag{9}$$

where

$$\widehat{\mathbf{A}}_E = \widehat{\mathbf{G}}_E \hat{\mathbf{e}}^{b,c}, \ \widehat{\mathbf{A}}_H = \widehat{\mathbf{G}}_H \hat{\mathbf{e}}^{b,c}, \tag{10}$$

$$\hat{\mathbf{C}} = \left(\hat{\mathbf{e}}^{b,c*} \hat{\mathbf{e}}^{b,c}\right)^{-1} \hat{\mathbf{e}}^{b,c*} \widehat{\mathbf{G}}_D \hat{\mathbf{e}}^{b,c}, \tag{11}$$

and diagonal matrix

$$\widehat{\mathbf{B}}(\mathbf{m}) = \left[\mathbf{diag}\left(\mathbf{I} - \widehat{\mathbf{C}}\mathbf{m}\right)\right]^{-1}. \tag{12}$$

We use the following notations in the last formulae. The vectors $\mathbf{e}^{a,r}$ and $\mathbf{h}^{a,r}$ represent the discrete quasi-analytical approximations of the anomalous electric field at the observation points. Vector $\mathbf{I}$ is a column vector of the length $N$ formed by units. Matrix $\widehat{\mathbf{e}}^{b,c}$ is a sparse tridiagonal $3N \times N$ matrix containing the $x$, $y$ and $z$ components of the primary (background) electric field at the centers of the cells of the anomalous domain $D$:

$$\widehat{\mathbf{e}}^{b,c} = \begin{bmatrix} E_x^{b,c1} & & \\ & \ddots & \\ & & E_x^{b,cN} \\ E_y^{b,c1} & & \\ & \ddots & \\ & & E_y^{b,cN} \\ E_z^{b,c1} & & \\ & \ddots & \\ & & E_z^{b,cN} \end{bmatrix}. \tag{13}$$

Matrices $\widehat{\mathbf{G}}_E$ and $\widehat{\mathbf{G}}_H$ are discrete analogs of the corresponding Green's tensors. These matrices consist of the elements of either the electric or the magnetic Green's tensor acting from the anomalous body to the receivers. $M$ is the number of receivers, and $N$ is the number of cells in the anomalous body. The number of rows in $\widehat{\mathbf{G}}_{E,H}$ equals the length of the data vector; $\widehat{\mathbf{G}}_{E,H}$ has $3N$ columns:

$$\widehat{\mathbf{G}}_{E,H} = \begin{bmatrix} G_{xx}^{11} & \cdots & G_{xx}^{1N} & G_{xy}^{11} & \cdots & G_{xy}^{1N} & G_{xz}^{11} & \cdots & G_{xz}^{1N} \\ & & & & \vdots & & & & \\ G_{xx}^{M1} & \cdots & G_{xx}^{MN} & G_{xy}^{M1} & \cdots & G_{xy}^{MN} & G_{xz}^{M1} & \cdots & G_{xz}^{MN} \\ G_{yx}^{11} & \cdots & G_{yx}^{1N} & G_{yy}^{11} & \cdots & G_{yy}^{1N} & G_{yz}^{11} & \cdots & G_{yz}^{1N} \\ & & & & \vdots & & & & \\ G_{yx}^{M1} & \cdots & G_{yx}^{MN} & G_{yy}^{M1} & \cdots & G_{yy}^{MN} & G_{yz}^{M1} & \cdots & G_{yz}^{MN} \\ G_{zx}^{11} & \cdots & G_{zx}^{1N} & G_{zy}^{11} & \cdots & G_{zy}^{1N} & G_{zz}^{11} & \cdots & G_{zz}^{1N} \\ & & & & \vdots & & & & \\ G_{zx}^{M1} & \cdots & G_{zx}^{MN} & G_{zy}^{M1} & \cdots & G_{zy}^{MN} & G_{zz}^{M1} & \cdots & G_{zz}^{MN} \end{bmatrix}.$$

Matrix $\widehat{\mathbf{G}}_D$ is a discrete analog of the corresponding electric Green's tensor acting

inside the domain $D$. We will call it *the domain scattering matrix.* It is the $3N \times 3N$ scattering matrix consisting of the elements of the electric Green's tensor inside the anomalous domain:

$$\widehat{\mathbf{G}}_D = \begin{bmatrix} G_{xx}^{11} & \cdots & G_{xx}^{1N} & G_{xy}^{11} & \cdots & G_{xy}^{1N} & G_{xz}^{11} & \cdots & G_{xz}^{1N} \\ & & & & \vdots & & & & \\ G_{xx}^{N1} & \cdots & G_{xx}^{NN} & G_{xy}^{N1} & \cdots & G_{xy}^{NN} & G_{xz}^{N1} & \cdots & G_{xz}^{NN} \\ G_{yx}^{11} & \cdots & G_{yx}^{1N} & G_{yy}^{11} & \cdots & G_{yy}^{1N} & G_{yz}^{11} & \cdots & G_{yz}^{1N} \\ & & & & \vdots & & & & \\ G_{yx}^{N1} & \cdots & G_{yx}^{NN} & G_{yy}^{N1} & \cdots & G_{yy}^{NN} & G_{yz}^{N1} & \cdots & G_{yz}^{NN} \\ G_{zx}^{11} & \cdots & G_{zx}^{1N} & G_{zy}^{11} & \cdots & G_{zy}^{1N} & G_{zz}^{11} & \cdots & G_{zz}^{1N} \\ & & & & \vdots & & & & \\ G_{zx}^{N1} & \cdots & G_{zx}^{NN} & G_{zy}^{N1} & \cdots & G_{zy}^{NN} & G_{zz}^{N1} & \cdots & G_{zz}^{NN} \end{bmatrix}.$$

Let us introduce a notation $\mathbf{d}$ for the electric or magnetic vector of the anomalous part of the observed data. This vector contains the components of the anomalous electric and/or magnetic fields at the receivers. Using these notations, the forward modeling problem for the electromagnetic field can be expressed by the following matrix operation:

$$\mathbf{d} = \widehat{\mathbf{A}} \left[ \mathbf{diag} \left( \mathbf{I} - \hat{\mathbf{C}}\mathbf{m} \right) \right]^{-1} \mathbf{m} = \widehat{\mathbf{A}}\hat{\mathbf{B}}(\mathbf{m})\, \mathbf{m}, \tag{14}$$

where $\widehat{\mathbf{A}}$ stands for the electric or magnetic matrices, $\widehat{\mathbf{A}}_E$ or $\widehat{\mathbf{A}}_H$, defined in (10).

## Quasi-analytical approximation for the magnetotelluric problem

In magnetotelluric (MT) and controlled source magnetotelluric (CSMT) methods the observed data are usually not recorded in a form of pure electric or magnetic field components. In particular, the results of magnetotelluric measurement are the *apparent resistivity* and *phase* calculated from the mutually orthogonal electric and magnetic field components. Let us denote an arbitrary horizontal electric field component by $E$, and define $H$ as the magnetic field component perpendicular to the direction of

$E$ at a particular receiver site. Note that both $E$ and $H$ are complex numbers. The *magnetotelluric impedance* is defined as the ratio of $E$ and $H$ :

$$Z = \frac{E}{H}. \tag{15}$$

Since the impedance does not depend on the actual strength of the source, it is a very practical parameter for natural electromagnetic field observations. The magnetotelluric apparent resistivity is calculated from $Z$, using

$$\rho = \frac{1}{cf}|Z|^2, \tag{16}$$

where $c = 2\pi\mu_0$. If the incident field is a plane-wave and the model is a homogeneous half-space, $\rho$ is equal to the true resistivity, making it indicative of the resistivity structure of the subsurface.

Another commonly measured parameter is the phase angle of the impedance:

$$\phi = \tan^{-1}\frac{ImZ}{ReZ}. \tag{17}$$

This quantity is less sensitive to the effect of shallow subsurface anomalies, so it is particularly useful for the detection of deep structures.

To obtain a simple relationship between the anomalous field components and the MT parameters, by taking into account that $E = E^b + E^a$ and $H = H^b + H^a$, the logarithm of $Z = E/H$ is expressed as

$$\ln Z = \ln\frac{E^b + E^a}{H^b + H^a} = \ln\left(\frac{E^b + E^a}{E^b}\cdot\frac{H^b}{H^b + H^a}\cdot\frac{E^b}{H^b}\right). \tag{18}$$

Thus,

$$\ln Z = \ln\left(1 + E^a/E^b\right) - \ln\left(1 + H^a/H^b\right) + \ln Z^b, \tag{19}$$

where $Z^b = E^b/H^b$ is the *background impedance.*

From equation (16)

$$\ln|Z| = \ln\left(cf\cdot\rho^{1/2}\right) = \ln(cf) + \frac{1}{2}\ln\rho. \tag{20}$$

The same relationship holds for the background impedance as well. Considering identities $\ln Z = \ln|Z| + i\phi$ and $\ln Z^b = \ln|Z^b| + i\phi^b$ results in

$$\frac{1}{2}\ln\rho^a + i\phi^a = \ln\left(1 + E^a/E^b\right) - \ln\left(1 + H^a/H^b\right), \tag{21}$$

where $\ln\rho^a = \ln\rho - \ln\rho^b$ is the *log anomalous apparent resistivity*, $\phi^a = \phi - \phi^b$ is the *anomalous phase*. Knowing the background cross-section, these quantities can be easily obtained from the measured total apparent resistivities and phases.

The log anomalous apparent resistivities and anomalous phases are organized into a data vector similar to (14):

$$\mathbf{d}^{MT} = \frac{1}{2}ln(\rho_a) + i\phi_a = ln\left[1 + \left(\widehat{\mathbf{e}}^{b,r}\right)^{-1}\mathbf{e}^{a,r}\right] - ln\left[1 + \left(\widehat{\mathbf{h}}^{b,r}\right)^{-1}\mathbf{h}^{a,r}\right], \tag{22}$$

where $\widehat{\mathbf{e}}^{b,r}$ and $\widehat{\mathbf{h}}^{b,r}$ are diagonal matrices containing the background electric and magnetic fields at the receivers:

$$\widehat{\mathbf{e}}^{b,r} = \begin{bmatrix} E^{b,r1} & & \\ & \ddots & \\ & & E^{b,rN} \end{bmatrix}, \quad \widehat{\mathbf{h}}^{b,r} = \begin{bmatrix} H^{b,r1} & & \\ & \ddots & \\ & & H^{b,rN} \end{bmatrix}, \tag{23}$$

and it is assumed that $ln$ is applied to each element of the corresponding vector.

Substituting the QA approximation in (8) and (9) into the vector of anomalous MT parameters in (22), the QA forward approximation for the data containing the log anomalous apparent resistivities and phases becomes

$$\mathbf{d}^{MT} = ln\left(\mathbf{k}_E\right) - ln\left(\mathbf{k}_H\right), \tag{24}$$

where

$$\begin{aligned} \mathbf{k}_E &= 1 + \left(\widehat{\mathbf{e}}^{b,r}\right)^{-1}\widehat{\mathbf{A}}_E\widehat{\mathbf{B}}(\mathbf{m})\mathbf{m}, \\ \mathbf{k}_H &= 1 + \left(\widehat{\mathbf{h}}^{b,r}\right)^{-1}\widehat{\mathbf{A}}_H\widehat{\mathbf{B}}(\mathbf{m})\mathbf{m}. \end{aligned} \tag{25}$$

To further simplify the MT forward operator, Portniaguine and Zhdanov (1999a) suggested linearizing expressions $\ln(1 + E^a/E^b)$ and $\ln(1 + H^a/H^b)$ by neglecting the

higher order terms in the power series expansion of the logarithmic function:

$$\ln(1+x) \approx x \quad \text{for small x.} \tag{26}$$

Thus, (24) becomes

$$\mathbf{d}_{lin}^{MT} = \widehat{\mathbf{A}}_{lin}^{MT} \hat{\mathbf{B}}(\mathbf{m})\ \mathbf{m}, \tag{27}$$

where

$$\widehat{\mathbf{A}}_{lin}^{MT} = \left[\left(\hat{\mathbf{e}}^{b,r}\right)^{-1}\widehat{\mathbf{G}}_E - \left(\hat{\mathbf{h}}^{b,r}\right)^{-1}\widehat{\mathbf{G}}_H\right]\hat{\mathbf{e}}^{b,c}. \tag{28}$$

The advantage of this expression is that the observed MT parameters can be expressed as a linear function of the anomalous electric and magnetic field components.

## Diagonalized quasi-analytical approximation

One can see that matrix $\widehat{\mathbf{C}}$ is responsible for the scattering inside the anomalous body, because it is determined by the domain scattering matrix $\widehat{\mathbf{G}}_D$ (see equation (11)). We can further simplify the quasi-analytical approximation by assuming that the anomalous electric field in a specific cell is affected mostly by the scattering in the same cell. In other words, we can simplify $\widehat{\mathbf{C}}$ by retaining its diagonal elements only. This is the basic idea of the *diagonalized quasi-analytical approximation* (DQA). The expressions of the anomalous electromagnetic and MT parameters are the same as (14), (24), and (27) for the QA approximation, except that formula (11) is replaced now by the following expression:

$$\widehat{\mathbf{C}} = \mathbf{diag}\left[\left(\hat{\mathbf{e}}^{b,c*}\hat{\mathbf{e}}^{b,c}\right)^{-1}\hat{\mathbf{e}}^{b,c*}\widehat{\mathbf{G}}_D\hat{\mathbf{e}}^{b,c}\right]. \tag{29}$$

To illustrate the accuracy of the DQA approximation, consider the following numerical experiment. The geoelectrical model consists of a rectangular conductive body with 10 ohm-m resistivity embedded in a homogeneous half-space with resistivity of 100 ohm-m (Figure 1). It is excited by a horizontal rectangular loop. The frequency is 1000 Hz.

The receivers are located above the body along the y axis. Figure 2 shows the real and imaginary parts of the horizontal electric and vertical magnetic components of the scattered field computed by solving the full integral equation and the QA and the DQA approximations. The accuracy of the diagonalized QA approximation is about the same as the QA approximation using the full matrix $\widehat{\mathbf{C}}$. Since the computational cost of the diagonal of $\widehat{\mathbf{C}}$ is $O(N)$ instead of $O(N^2)$, the calculation of the DQA approximation is practically the same as the Born approximation.

# Tikhonov regularization in the solution of inverse problems

In the previous section we defined quick forward operators for modeling anomalous fields and magnetotelluric parameters in the presence of three-dimensional model geometry. In general, these formulae can be expressed by a vector-vector operator equation including the data vector $\mathbf{d}$ and the vector of model parameters $\mathbf{m}$ as

$$\mathbf{d} = \mathbf{G}(\mathbf{m}), \tag{30}$$

where $\mathbf{G}$ is the forward operator symbolizing the governing equations of the EM modeling problem.

Inversion aims to determine the model parameter vector $\mathbf{m}$ based on $\mathbf{G}$ and a known (observed) data vector $\mathbf{d}$:

$$\mathbf{m} = \mathbf{G}^{-1}(\mathbf{d}). \tag{31}$$

This problem is usually ill-posed, i.e., the solution can be nonunique and unstable. The conventional way of solving ill-posed inverse problems, according to regularization theory (Tikhonov and Arsenin, 1977, Zhdanov, 1993), is based on minimization of the Tikhonov parametric functional:

$$P(\mathbf{m}) = \phi(\mathbf{m}) + \alpha S(\mathbf{m}) = min, \tag{32}$$

where $\phi(\mathbf{m}) = ||\mathbf{G}(\mathbf{m}) - \mathbf{d}||_2^2$ is the misfit functional between the theoretical values $\mathbf{G}(\mathbf{m})$ and the observed data $\mathbf{d}$, $s(\mathbf{m})$ is a stabilizing functional, and $\alpha$ is a regularization parameter. The optimal value of $\alpha$ is determined from the misfit condition,

$$\varphi(\mathbf{m}) = \delta_d, \tag{33}$$

where $\delta_d$ is the noise level of the data.

Note that the traditional way to implement regularization in inverse problem solution is based on considering the class of inverse models with smooth distribution of the model parameters (Constable et al., 1987). Within the framework of the classical Tikhonov regularization, one can select the smooth solution by introducing the corresponding minimum norm, or "smoothing" stabilizing functionals. This approach is widely used in geophysics and is proven to be a powerful tool for stable inversion of geophysical data. Most MT inversion methods use the same approach, resulting in a smooth image of geoelectrical structures.

The traditional inversion algorithms providing smooth solutions for geoelectrical structures have difficulties, however, in detecting sharp geoelectrical boundaries between different geological formations. This problem arises, for example, in inversion for the local conductive target with sharp boundaries between the conductor and the resistive host rocks, which is a typical model in mining exploration. In these situations, it can be useful to search for a stable solution within the class of inverse models with sharp geoelectrical boundaries.

The mathematical technique for solving this problem was developed by Portniaguine and Zhdanov (1999b). It is based on introducing a new type of stabilizing functional in inverse problem solution, the so-called minimum support or minimum gradient support functionals. We call this technique a focusing regularized inversion to distinguish it from the traditional smooth regularized inversion.

The minimization problem (32) can be solved using any gradient type technique. We use the re-weighted regularized conjugate gradient (RRCG) method. Implementation details of this algorithm are specified in Zhdanov and Hursán (2000) and Zhdanov (2001).

# Frechet derivatives

A critical point of a gradient-type inversion algorithm is the calculation of the Frechet derivative (sensitivity) operator $\mathbf{F}$ at every iteration of the RRCG method. In this section we recall first the Frechet dericatives of anomalous field data introduced by Zhdanov and Hursán (2000). Then, we derive the sensitivity operators for the magnetotelluric problem.

## Frechet derivative matrix for anomalous field data

In the derivation of the Frechet derivative matrix of the forward operator (14) taking into account that the model parameters are the anomalous conductivity values in the cells of the anomalous body, matrix $\widehat{\mathbf{A}}$ is independent of the model parameters, and $\widehat{\mathbf{B}}$ is a diagonal matrix, one can express the perturbation of the forward operator (14) with respect to the vector of model parameters in the form

$$\delta \mathbf{d} = \widehat{\mathbf{A}}\ \delta \left[\widehat{\mathbf{B}}(\mathbf{m})\ \mathbf{m}\right] = \widehat{\mathbf{A}}\ \left\{\widehat{\mathbf{B}}(\mathbf{m})\delta\mathbf{m} + diag(\mathbf{m})\delta\left[\widehat{\mathbf{B}}(\mathbf{m})\right]\right\}. \tag{34}$$

Since

$$\begin{aligned} &\delta\left[\widehat{\mathbf{B}}(\mathbf{m})\right] = \delta\left[diag\left(\mathbf{I}-\widehat{\mathbf{C}}\mathbf{m}\right)\right]^{-1} = \\ &\left[diag\left(\mathbf{I}-\widehat{\mathbf{C}}\mathbf{m}\right)\right]^{-2}\ \widehat{\mathbf{C}}\ \delta\mathbf{m} = \widehat{\mathbf{B}}^2(\mathbf{m})\ \widehat{\mathbf{C}}\ \delta\mathbf{m}, \end{aligned} \tag{35}$$

the result is

$$\delta\mathbf{d} = \widehat{\mathbf{A}}\ \left\{\widehat{\mathbf{B}}(\mathbf{m}) + diag(\mathbf{m})\widehat{\mathbf{B}}^2(\mathbf{m})\ \widehat{\mathbf{C}}\right\}\delta\mathbf{m} = \widehat{\mathbf{F}}(\mathbf{m})\ \delta\mathbf{m}, \tag{36}$$

where

$$\widehat{\mathbf{F}}(\mathbf{m}) = \widehat{\mathbf{A}}\ \widehat{\mathbf{D}}(\mathbf{m}) \tag{37}$$

is the Frechet derivative matrix, and $\widehat{\mathbf{D}}$ is a diagonal matrix:

$$\widehat{\mathbf{D}}(\mathbf{m}) = \hat{\mathbf{B}}(\mathbf{m}) + diag(\mathbf{m})\hat{\mathbf{B}}^2(\mathbf{m})\ \hat{\mathbf{C}}, \tag{38}$$

and $diag(\mathbf{m})$ denotes a diagonal matrix formed by the elements of the vector $\mathbf{m}$.

One can see that in the framework of DQA approximation, matrix $\hat{\mathbf{F}}$ is the product of $\widehat{\mathbf{A}}$ and a diagonal matrix $\widehat{\mathbf{D}}$. The numerical computations based on formula (37) are very fast and efficient, because the full matrix $\widehat{\mathbf{A}}$ and diagonal matrix $\hat{\mathbf{C}}$ do not depend on the variable model parameter, so they are precomputed and fixed during the inversion. Only vector $\mathbf{m}$ and diagonal matrix $\hat{\mathbf{B}}(\mathbf{m})$ are updated on each iteration of the inverse process. Thus, the cost of matrix multiplications involving $\hat{\mathbf{F}}$ is essentially the same as the multiplication with $\widehat{\mathbf{A}}$ which means that the DQA inversion is almost as inexpensive as the Born inversion. However, it is shown below that it produces more accurate results than the Born inversion, because it takes into account the nonlinear effects in the observed EM data.

## Frechet derivative matrix for magnetotelluric data

Considering identity $\delta_{\mathbf{m}}\left[ln\left(\mathbf{f}(\mathbf{m})\right)\right] = \left[diag\left(\mathbf{f}(\mathbf{m})\right]^{-1}\delta_{\mathbf{m}}\left(\mathbf{f}(\mathbf{m})\right)\right.$ for perturbation of vector operators, the perturbation of forward operator (24) with respect to the model parameter vector $\mathbf{m}$ may be expressed as

$$\delta_{\mathbf{m}}\left[\mathbf{d}^{MT}(\mathbf{m})\right] = \left\{diag\left[\mathbf{k}_E(\mathbf{m})\right]\right\}^{-1}\delta_{\mathbf{m}}\left[\mathbf{k}_E(\mathbf{m})\right] - \left\{diag\left[\mathbf{k}_H(\mathbf{m})\right]\right\}^{-1}\delta_{\mathbf{m}}\left[\mathbf{k}_H(\mathbf{m})\right] \tag{39}$$

The perturbation $\delta_{\mathbf{m}}\left[\mathbf{k}_E(\mathbf{m})\right]$ can be expressed as

$$\delta_{\mathbf{m}}\left[\mathbf{k}_E(\mathbf{m})\right] = \left(\hat{\mathbf{e}}^{b,r}\right)^{-1}\widehat{\mathbf{A}}_E\ \delta_{\mathbf{m}}\left[\hat{\mathbf{B}}(\mathbf{m})\mathbf{m}\right] = \left(\hat{\mathbf{e}}^{b,r}\right)^{-1}\ \widehat{\mathbf{A}}_E\ \widehat{\mathbf{D}}(\mathbf{m})\ \delta_{\mathbf{m}}\mathbf{m}, \tag{40}$$

where $\widehat{\mathbf{A}}$ stands for the electric or magnetic matrices used in equation (14). A similar expression can be obtained for $\delta_{\mathbf{m}}\left[\mathbf{k}_H(\mathbf{m})\right]$ as well. Combining (39) and (40) finally gives

$$\delta_{\mathbf{m}}\left[\mathbf{d}^{MT}(\mathbf{m})\right] = \widehat{\mathbf{A}}^{MT}(\mathbf{m})\ \widehat{\mathbf{D}}(\mathbf{m})\ \delta_{\mathbf{m}}\mathbf{m}, \tag{41}$$

where

$$\widehat{\mathbf{A}}^{MT}(\mathbf{m}) = \{diag\,[\mathbf{k}_E(\mathbf{m})]\}^{-1}\left(\widehat{\mathbf{e}}^{b,r}\right)^{-1}\widehat{\mathbf{A}}_E - \{diag\,[\mathbf{k}_H(\mathbf{m})]\}^{-1}\left(\widehat{\mathbf{h}}^{b,r}\right)^{-1}\widehat{\mathbf{A}}_H. \qquad (42)$$

Thus, the Frechet derivative matrix for the magnetotelluric forward problem (22) is

$$\widehat{\mathbf{F}}^{MT}(\mathbf{m}) = \widehat{\mathbf{A}}^{MT}(\mathbf{m})\;\widehat{\mathbf{D}}(\mathbf{m}). \qquad (43)$$

Note that in the case of DQA approximation the terms depending on the model parameters are diagonal matrices in (42). Therefore, similarly to the case of anomalous field inversion, the iterative updating of $\widehat{\mathbf{F}}^{MT}(\mathbf{m})$ is relatively inexpensive during the inversion process. The operational cost of a matrix multiplication with $\widehat{\mathbf{F}}^{MT}(\mathbf{m})$ is approximately four matrix multiplications involving full matrices $\widehat{\mathbf{A}}_E$ and $\widehat{\mathbf{A}}_H$.

The linearized operator (27) provides an even simpler Frechet operator. Since matrix $\widehat{\mathbf{A}}_{lin}^{MT}$ does not depend on $\mathbf{m}$, the derivation is identical to that considered in obtaining the Frechet matrix of anomalous field data. Thus,

$$\widehat{\mathbf{F}}_{lin}^{MT}(\mathbf{m}) = \widehat{\mathbf{A}}_{lin}^{MT}\;\widehat{\mathbf{D}}(\mathbf{m}). \qquad (44)$$

Besides the simpler formulation, one multiplication by the Frechet matrix costs two Green's matrix multiplications only, providing an algorithm twice as fast as that using the full expression (43). Test inversions of synthetic data demonstrated that this approximation also produces adequately accurate inverse models.

Once the forward operator with the corresponding Frechet matrices and the minimization scheme are implemented, an inversion can be successfully performed. However, there is a possibility of further improvements by exploiting properties specific to our particular inverse problem.

In the case of integral-based electromagnetic inverse problems, we consider the following: 1) the layered Green's functions exhibit convolution properties, 2) the total conductivity must be always positive in the predicted model.

In Appendix A we show that using horizontally homogeneous model discretization one can drastically reduce the memory and CPU time requirements of the Green's matrix manipulations by employing the convolution theorem. Also, in Appendix B we demonstrate the possibility of using the logarithm of the total conductivity as a model parameter ensuring realistic inverse models.

## Model study

Consider a homogeneous half-space with resistivity of 100 ohm-m, containing a conductive (10 ohm-m) dipping dike. The top of the anomaly is 100 m, and its bottom is 600 m beneath the surface. This model is excited by plane EM waves at four different frequencies: 1, 10, 100 and 1000 Hz. The theoretical observed field was calculated in the nodes of a rectangular grid at the surface by solving the full integral equation. The distance between the observation points is 100 m in the X and Y directions. The three-dimensional sketch of the true model with the inverted area and the receiver points is shown in Figure 3a.

Following the traditional approach used in practical MT observations, synthetic observed apparent resistivities and phases were calculated based on two off-diagonal elements of the magnetotelluric impedance tensor at each observation point. The quantities $\rho_{yx}$ and $\phi_{yx}$ are assigned to the nominal TE mode, whereas $\rho_{xy}$ and $\phi_{xy}$ are assigned to the nominal TM mode. Note that this 2-D nomenclature is artificial and approximate in nature for 3-D structures. However, it is widely used in practical MT observations, and usually only the quantities $\rho_{yx}$, $\phi_{yx}$, $\rho_{xy}$ and $\phi_{xy}$ are available for inversion. That is why the same approach is used in the model study.

The inverted area is a homogeneous mesh consisting of $15 \times 13 \times 9$ cubic cells surrounding the anomalous structure to be inverted. Each cell has a dimension of 100 m in the x, y and z directions. The inverted area is also shown in Figure 3a. The

vertical slices of the inverted area with the true model are presented in Figure 3b.

The data vector consists of 1560 simulated field components. The synthetic data have been contaminated by 3 percent random noise. The model parameters are the conductivity values of each cell of the inverted area. Diagonalized quasi-analytical (DQA) inversions were performed using smooth and focusing regularizations using the exact and linearized magnetotelluric forward operators introduced by equations (24) and (27), respectively. Here "exact" means that the MT parameters are not approximated, however, the DQA approximation for the anomalous field solutions is still used. Figures 4 and 5 show the results of inversions for the full and linearized MT forward operators, respectively. We performed inversions by considering single TE and TM mode data as well as joint inversion of both TE and TM modes.

The results of the smooth inversion of single TE and single TM mode data using the exact MT operator are shown in Figures 4a and 4c, correspondingly. Like in the previous examples, the image has spread around the location of the inhomogeneity with an underestimated conductivity contrast. However, one can see the inclination of the dike even in this smooth image. Note that the inversion of single TM mode data produces a better image of the conductive target than the TE mode inversion.

The focusing DQA inversion produces a sharper and clearer image of the dike (Figures 4b and 4d). However, the resolution of the TM mode inversion is again much better than in the case of TE mode inversion, which corresponds well to the known result published by Wannamaker (1999). In the case of the TE mode, the primary electric field is polarized along the strike direction, and therefore, it is less sensitive to the dike boundaries parallel to the strike. In the case of the TM mode, the primary electric field is directed across the strike, and it becomes more sensitive to the dike boundaries.

Figures 4e and 4f present the results of joint TE and TM mode smooth and

focusing inversion. Both images provide a reasonable reconstruction of the position and inclination of the dike. However, the smooth image is, naturally, more diffuse and underestimates the conductivity of the dike, while the focusing inversion provides clearer and more correct image of the conductive target. Generally, the best result is obtained if the TM mode (when the electric field is perpendicular to the direction of the strike) is measured. In realistic situations, however, when the strike direction is unknown, the joint inversion of both modes might be necessary. The joint inversion provides a reasonable image without knowing the orientation of the target.

As can be seen in Figure 5, the linearized MT forward operator produces similar pictures for all inversions. Thus, for large scale inversions the linearized MT operator is preferable because it requires only half the memory and CPU time.

For comparison, the results of the smooth and focusing Born inversions with the exact MT operator are shown in Figures 6a and 6b respectively, for joint TE and TM mode data. This model is severely underestimates the size and the conductivity of the anomaly. The DQA inversion can resolve three-dimensional conductive targets much better than the Born inversion. At the same time, the computational resources (computer memory and CPU time) required for DQA inversion are practically the same as for the Born inversion. That is why this method is called a *rapid 3-D electromagnetic inversion.*

## Case studies

The ultimate test for a new inversion method is the interpretation of real measurements. Three 3-D data sets were available for our inversion algorithm.

The first experiment is the inversion of a dense array magnetotelluric data set collected by Takasugi et al. (1992) over the Minamikayabe area, Japan. This area is important mainly because of its geothermal potential and it has been extensively

examined by different geophysical methods. Rapid three-dimensional inversion was performed using both smooth and focusing stabilizers. The inversion results coincide with the preexisting geological information and independent EM interpretations.

The second case study involves interpretation of the results of an array magnetotelluric survey consisting of eleven profiles covering an area of about 28 $km^2$, collected by INCO Exploration at the Voisey's Bay area, where massive sulfide deposits were discovered (Naldrett et al., 1996). A massive inversion consisting of 2760 data and 33600 model parameters was computed in less than 15 minutes.

All inversions were extremely fast compared to other techniques. In case of a couple of hundreds or a few thousand unknown model parameters the speed was approximately 10-30 times higher than the QL inversion scheme, while in the case of the third experiment, where there were above thirty thousand cells, no other method could be used on a PC-range computer.

## Inversion of the Minamikayabe area data

The New Energy and Industrial Technology Development Organization (NEDO) has been conducting a "Geothermal Development Promotion Survey" in the Minamikayabe area located in the southern part of Hokkaido, Japan (Takasugi et al., 1992). This area is particularly interesting because of its geothermal potential. It is characterized by a resistive magmatic intrusion surrounded by fractured host rocks with relatively high conductivity. In 1988, MT sounding and AMT soundings were conducted in this area with site spacing of 100 m along and across observational profiles (Figure 7). The frequency range of MT data is from 1 Hz to 130 Hz. Because the survey area at Minamikayabe is located very close to Uchiura Bay on the northeastern side, low frequency data are strongly affected by the "coast effect" (Takasugi et al., 1992). Also, we are interested in shallow geological structure in this area, so it

is reasonable to restrict ourselves to frequencies which are greater than 1 Hz so that the coast effect can be neglected. We use MT data for inversion at seven different frequencies between 1 Hz and 100 Hz (96 Hz, 48 Hz, 24 Hz, 12 Hz, 6 Hz, 3 Hz, and 1.5 Hz). The selected background model is similar to one used for QL inversion (Zhdanov et al., 2000a). It was refined to a four layer model with resistivities of 480 ohm-m, 6 ohm-m, 15 ohm-m and 270 ohm-m, and corresponding thicknesses of 30 m and 450 m and 200 m.

Both nominal TE mode and TM mode data for a total of 161 MT soundings were used in the inversion. The sketch of a typical cross-section below the center of the inverted area, based on 2-D interpretation of MT data (according to Takasugi et al., 1992) is shown in Figure 8. The inverted area was divided into 26 $\times$ 26 cells horizontally (each cell has a 50 m $\times$ 50 m size in the x and y directions), and 11 layers in the vertical direction (Figure 7b). The vertical cell sizes are 25 m for the first layer, 50 m for the next seven layers and 100 m for the cells at the bottom three layers. The cell sizes increase with depth.

The CPU time for the rapid 3-D MT inversion was about 10 minutes using a Sun Ultra Sparc 10 workstation. The total number of iterations was about 40. Figure 9a-b shows the volume images of the models predicted by smooth and focusing DQA inversions, respectively. The vertical cross-sections of the smooth and focusing inversion results can be seen in Figures 10a-b, respectively. The inversion results are consistent with the 2-D interpretation results by Takasugi et al., (1992), shown in Figure 8, and with 3-D inversion results obtained by QL inversion (Zhdanov et al., 2000a).

The comparisons of observed and predicted TM mode apparent resistivities and phases at four profiles are presented in Figures 11a-d. They show good agreement between the observed and predicted apparent resistivity and phase pseudo-sections.

## Inversion of the Voisey's Bay data

INCO Exploration conducted a three-dimensional MT survey in the Voisey's Bay area. The goal of this survey was studying the application of the MT method to typical Ni-Cu-Fe sulfide mineralization zone exploration in complex geological structures (Naldrett et al., 1996; Balch, 2000).

The deposits are hosted by troctolite dikes that are thought to be feeder conduits for the Voisey's Bay intrusion of the Nain Plutonic Suite (Naldrett et al., 1996). The Western Extension, which includes the Reid Brook and Discovery Hill deposits, is a near-vertical troctolite dike over 3 km in strike length, extending from near-surface to almost 2 km at depth, where it remains open. Mineralization within the dike is composed of lenses of disseminated and semi-massive to massive sulfide. The Ovoid deposit is located under 20 m of overburden at the eastern end of the Western Extension and is 70% massive sulfide. The Eastern Deeps deposit is located at the mouth of a feeder dike along the entry point where the dike opens into a large troctolite magma chamber. The overlying troctolite of the Eastern Deeps deposit is barren of sulfide in the upper 300-400 m at the western margin and in the upper 800-1000 m near the eastern limit.

The Voisey's Bay Troctolite is shown on the Nain Block geology map (Figure 12, top panel). There is a strong correlation between the known mineralization zones and the total magnetic field (Figure 12, bottom panel). The Enderbitic Orthogneiss and Nain Gneiss units are strongly magnetic, while the Tsiuayak Gneiss, the Makhavinekh and Voisey's Bay Granites, and the Voisey's Bay and Sarah Troctolites are mostly non-magnetic (Balch et al., 1998).

Note that the typical Ni-Cu-Fe sulfide mineralization in the Voisey's Bay Ni-Cu-Co deposits is composed mainly of pyrrhotite, pentlandite, and chalcopyrite. Pyrrhotite

has a high conductivity ranging from $10^4$ to $10^6$ S/m.

Pyrrhotite can be magnetic, so the EM responses can be used in an attempt to separate sulfide conductors from conductive graphite. However, graphitic rock units can contain magnetite and will also produce a magnetic response.

The area lies very close to the sea. This means that the groundwater has variable salt concentration resulting in a significant alteration of the resistivity structure. In order to be able to find anomalies due to the relatively small conductive ore deposits, it is extremely critical to delineate the regional resistivity anomalies caused mainly by the presence of saline groundwater. Since the transition zone between the fresh and saline waters can have a complicated structure, it was desirable to perform regional three-dimensional EM measurements targeting a depth range of about one kilometer.

The boundaries of the magnetotelluric survey are shown in Figure 12 by a bold dashed line. The 3-D MT survey consists of eleven lines passing from the South to the North. The frequency range of MT data is from 10 Hz to 350 Hz. We chose MT data for inversion at five different frequencies between 32 Hz and 288 Hz (288Hz, 166Hz, 95Hz 55Hz and 32Hz).

The simple analysis of the apparent resistivity and phase curves showed the presence of an anomaly zone between profiles number six and eleven. The MT profiles are numbered from the left to the right in Figure 13. For example, Figure 13 presents the maps of TE mode apparent resistivity (top panel) and phase (bottom panel) for a frequency of 96 Hz. We can see clearly the location of the anomalous zone in these maps.

For detailed investigation we used data from the six profiles in the eastern part crossing the anomalous zone. The background geoelectrical cross-section in this area, according to the MT data, was represented by a seven-layer model with the following resistivity-sequence: $\rho_1 = 305$, $\rho_2 = 283$, $\rho_3 = 452$, $\rho_4 = 461$, $\rho_5 = 607$, $\rho_6 = 452$, $\rho_7 =$

556; $h_1 = 100$, $h_2 = 200$, $h_3 = 200$, $h_4 = 100$, $h_5 = 100$, $h_6 = 200$. This cross-section has been found using the parameter-estimation code developed by Portniaguine and Zhdanov (1995). The inverted area consists of 33600 ($56 \times 50 \times 12$) cells. Figure 14 presents the 3-D view of the inverted area and its discretization. The structure of the MT stations is a little bit irregular. The MT data (apparent resistivities and phases) were interpolated in the six profiles shown in Figure 14.

The rapid 3-D MT inversion method was applied to joint TE and TM mode data for the 276 interpolated MT soundings at five frequencies.

Since the majority of the anomalies are attributed to the transition zones between groundwaters of different salinities, it is reasonable to suppose that the smooth inversion produces realistic images of the conductivity structures.

As a result of the inversion, we obtained a volume distribution of electrical resistivity under the area of about 28 $km^2$ to a depth of 1 km. In Figure 15a we can see the vertical cross-sections of the inverse results below the observation profiles. Figure 15b presents the general 3-D view of the predicted model. The top panel in Figure 16 shows 3-D conductive bodies with resistivity below 25 ohm-m, while the bottom panel presents the domains with resistivity below 50 ohm-m. One can see a conductive anomaly with a complex shape in these Figures, reaching a depth of several hundred meters.

The observed and predicted apparent resistivities and phases are shown in Figure 17a-d. Generally, the apparent resistivities show better agreement than the phases.

The images obtained by the rapid inversion scheme correspond well to the results obtained earlier by QL inversion using a coarser model discretization (Golubev and Zhdanov, 2000). However, the original QL inversion for this model required several hours of CPU time, while the rapid 3-D MT inversion runs for just about 14 minutes. The results were been achieved at approximately 30 iterations.

# Conclusions

We have demonstrated in this paper that the quasi-analytical approximation, developed by Zhdanov et al. (2000b) and Zhdanov and Hursán (2000) can be effectively used for 3-D inversion of the array magnetotelluric data. The important modifications of the QA approximations, introduced in this paper, including a diagonalized form of QA approximation and fast Green's tensor calculations, make the developed technique extremely fast and efficient.

The CPU time was measured during the inversions of synthetic and real data on a Sun Ultra Sparc 10 workstation. The numbers of data and model parameters with the execution time are listed in Table 1. One can see that the runtime remains less than 15 minutes even in the case of several thousands of model parameters and data enabling the user to perform several inversion attempts on massive data sets with different inversion parameters.

The practical use of the inversion algorithm was demonstrated on the inversion of real data sets. The results were consistent with pre-existing geological information and independent interpretations. The fine discretizations provided more detailed geoelectrical images than previous results. The new inversion results helped a better geological understanding of the inverted areas. The speed of the rapid inversion is superior to existing algorithms, making it a useful tool for practical applications.

# Acknowledgments

The authors acknowledge the support of the University of Utah Consortium for Electromagnetic Modeling and Inversion (CEMI), which includes AGIP, Baker Atlas Logging Services, BHP Minerals, ExxonMobil Upstream Research Company, INCO Exploration, International Energy Services, Japan National Oil Corporation, MIN-

DECO, Naval Research Laboratory, Rio Tinto-Kennecott, Sumitomo Metal Mining Co., and 3JTech Corporation.

We are thankful to Dr. Takasugi, GERD, Japan for the Minamikayabe area data.

Special thanks to INCO Exploration, and in particular to Drs. Alan King and Steve Balch, for providing MT data, collected for mining exploration, and permission to publish the inversion results.

# References


Alumbaugh, D. L., and Newman, G. A., 1997, Three-dimensional massively parallel inversion - II. Analysis of a cross-well electromagnetic experiment: Geophys. J. Int., **128**, 355-363.

Balch, S. J., 2000, Geophysics in mineral exploration: fundamentals and case histories. Ni-Cu sulphide deposits with examples from Voisey's Bay: in Practical Geophysics III, Northwest Mining Association.

Balch, S. J., Crebs, T. J., King, A., and Verbiski M., 1998, Geophysics of the Voisey's Bay Ni-Cu-Co Deposits: 68th Ann. Mtg. Soc. Expl. Geophys., Expanded Abstracts, 784-787.

Born, M., 1933, Optics: Springer-Verlag New York, Inc.

Constable, S. C., Parker, R. C., and Constable, C. G., 1987, Occam's inversion: a practical algorithm for generating smooth models from EM sounding data: Geophysics, **52**, 289-300.

Eaton., P. A., 1989, 3-D EM inversion using integral equations: Geophysical Prospecting, **37**, 407-426.

Golubev, N. G. and Zhdanov, M. S., 2000, Three-dimensional interpretation of magnetotelluric data collected for mineral exploration in Voisey's Bay, Labrador, Canada: Proceedings of 2000 CEMI Annual Meeting, 559-594.

Golubev, N., Zhdanov, M. S., Matsuo, K., and Negi, T., 1999, Three-dimensional inversion of magnetotelluric data over Minami-Noshiro oil field: Second International Symposium of Three-Dimensional Electromagnetics, University of Utah, 305-308.

Habashy, T. M., Groom, R. W., and Spies, B. R., 1993, Beyond the Born and Rytov approximations: J. Geophys. Res., **98**, 1759-1775.

Hohmann, G. W., 1975, Three-dimensional induced polarization and EM modeling: Geophysics, **40**, 309-324.

Hursán, G., 2001, Storage reduction and fast matrix multiplication integral-based geophysical problems: Proceedings of 2001 CEMI Annual Meeting, 17-38.

Madden, T. R., and Mackie, R. L., 1989, 3-D magnetotelluric modelling and inversion: Proceedings of the IEEE, **77**, 318-332.

Naldrett, A. J., Keats, H., Sparkes, K., and Moore S., 1996, Geology of the Voisey's Bay Ni-Cu-Co Deposit, Labrador, Canada: Explor. Mining Geol., **5**, 169-179.

Newman, G. A., and Alumbaugh, D. L., 1996, 3-D EM modeling and inversion on massively parallel computers: Sandia Report, SAND96-0582.

Newman, G. A., and Alumbaugh, D. L., 1997, Three-dimensional massively parallel inversion - I. Theory: Geophys. J. Int., **128**, 355-363.

Portniaguine O., and M. S. Zhdanov, 1995, Parameter estimation method in the solution of multi-dimensional geo-electromagnetic inverse problems: 3-D electromagnetics: Proceeding of the First International Symposium on Three-Dimensional Electromagnetics, Schlumberger-Doll Research, Ridgefield, CT.

Portniaguine, O. N., and Zhdanov, M. S., 1999a, 3-D focusing inversion of CSMT data: Proceeding of the Second International Symposium on Three-Dimensional Electromagnetics, University of Utah, Salt Lake City, 132-135.

Portniaguine, O. N., and Zhdanov, M. S., 1999b, Focusing geophysical inversion images: Geophysics, **64**, 874-887.

Smith, J. T., and Booker, J. R., 1991, Rapid inversion of 2 and 3-D magnetotelluric data: J. Geophys. Res., **96**, 3905-3922.

Takasugi S., Keisaku T., Noriaki K., and Shigeki, M., 1992, High spatial resolution

of the resistivity structure revealed by a dense network MT measurement – a case study in the Minamikayabe area, Hokkaido, Japan: J. Geomag. Geoelectr., **44**, 289-308.

Tikhonov, A. N. and Arsenin, V. Y., 1977, Solution of ill-posed problems: V. H. Winston and Sons, Washington D. C.

Torres-Verdin, C. and Habashy T. M., 1994, Rapid 2.5-dimensional forward modeling and inversion via a new nonlinear scattering approximation: Radio Sci., **29**, 1051-1079.

Wannamaker, P. E., 1999, Affordable magnetotellurics: Interpretation in Natural Environments: in Three-Dimensional Electromagnetics, edited by Michael Oristaglio and Brian Spies, SEG publication.

Wannamaker, P. E., 2000, Resolution principles of diffusive EM applied to 2-D MT inversion using a-priori constraints: Proceeding of the CEMI 2000 Annual Meeting, 253-282.

Weidelt, P., 1975, EM induction in three-dimensional structures: J. Geophysics, **41**, 85-109.

Zhdanov, M. S., 1993, Tutorial: regularization in inversion theory: Colorado School of Mines, 47 pp.

Zhdanov, M. S., 2001, Geophysical Inverse Theory and Regularization Problems, Elsevier, Amsterdam, in press.

Zhdanov M. S., Dmitriev, V. I., Fang, S., and Hursán, G., 2000b, Quasi-analytical approximations and series in electromagnetic modeling: Geophysics, **65**, 1746-1757.

Zhdanov, M. S, and Fang, S., 1996, 3-D quasi-linear electromagnetic inversion: Radio

Sci., **31**, 741-754.

Zhdanov, M. S., and Fang, S., 1997, Quasi-linear series in three-dimensional electromagnetic modeling: Radio Sci., **32**, 2167-2188.

Zhdanov, M. S. and Fang, S., 1999, 3D quasi-linear electromagnetic modeling and inversion: Three Dimensional Electromagnetics, SEG Monograph, 233-255.

Zhdanov, M. S., Fang, S., and Hursán, G., 2000a, Electromagnetic inversion using quasi-linear approximation: Geophysics, **65**, 1501-1513.

Zhdanov, M. S., and Hursán, G., 2000, 3-D electromagnetic inversion based on quasi-analytical approximation: Inverse Problems, **16**, 1297-1322.

Zhdanov, M. S., and Keller, G. W., 1994, The geoelectrical methods in geophysical exploration: Elsevier, Amsterdam-London-New York-Tokyo, 873 pp.

# Appendix A – Fast Green's tensor calculations based on the convolution and FFT method

For simplicity let us consider forward operator (14). It can be represented in a form of

$$\mathbf{d} = \widehat{\mathbf{G}}_{E,H}\, \mathbf{j}_a, \tag{A–1}$$

where $\widehat{\mathbf{G}}_{E,H}$ stands for the matrix of electric or magnetic Green's tensors acting from the anomalous domain to the receiver, and

$$\mathbf{j}_a = \widehat{\mathbf{e}}^{b,c}\, \widehat{\mathbf{B}}(\mathbf{m})\, \mathbf{m} \tag{A–2}$$

is the vector of scattering currents inside the anomalous domain based on the QA or DQA approximation.

It can be easily shown that if the anomalous domain is discretized into a horizontally homogeneous array of cells and the receivers coincide with this grid in horizontal directions, the Green's matrix has a block Toeplitz structure. In this case the number of different entries is much less than the total number of elements of the matrix, providing a good opportunity for economic storage. More specifically, the size of the Green's tensor kernels (the arrays storing all different matrix values) is $N_x \times N_y$ times smaller than the number of the elements in the original matrix. Here $N_x$ and $N_y$ stand for the number of cells in $x$ and $y$ directions, respectively. For example, if we discretize the anomalous body by a $20 \times 20$ grid in horizontal directions, the number of elements to be stored in the Green's tensor kernels is 400 times smaller than the size of the Green's matrix.

Moreover, this property provides not only an economical storage, but an effective computational tool as well. It can be shown that the multiplication with $\widehat{\mathbf{G}}_{E,H}$ can be represented as a sequence of discrete 2-D convolutions. Following the notations in

Hursán (2001), the schematic form of this operation can be summarized as

$$\mathbf{d} = \widehat{\mathbf{G}}_{E,H}\, \mathbf{j}_a = \mathbf{g} * \mathbf{j}_a, \tag{A–3}$$

where $\mathbf{g}$ is an array of Green's tensor kernels, and $*$ stands for the convolution operator. Therefore, we can apply the discrete convolution theorem

$$\mathbf{d} = FFT^{-1}\left[FFT(\mathbf{g}) \cdot FFT(\mathbf{j}_a)\right]. \tag{A–4}$$

The advantage of using this equation is that we replace the direct Green's matrix multiplication with the Fast Fourier transforms reducing the operation complexity from $O(N^2)$ into $O(NlogN)$.

# Appendix B – The logarithm of the total conductivity as a model parameter

We have introduced above the formulation of the electromagnetic inverse problem with respect to the anomalous conductivity vector, denoted by $\mathbf{m}$. However, during the minimization anomalous conductivity values resulting in negative total conductivity can occur. Thus, the anomalous conductivity must be transformed into a new space of model parameters with the property that the total conductivity always remains positive. The conventional way to solve this problem is to use the logarithm of the total conductivity as a model parameter:

$$\widetilde{\mathbf{m}} = ln(\sigma_b + \mathbf{m}). \tag{B–1}$$

Obviously, this model parameter can never produce negative conductivity. The inverse transform is

$$\mathbf{m} = exp(\widetilde{\mathbf{m}}) - \sigma_b. \tag{B–2}$$

To calculate the Frechet derivative with respect to this new model parameter, the forward operator is rewritten in terms of $\widetilde{\mathbf{m}}$:

$$\mathbf{d}(\widetilde{\mathbf{m}}) = \mathbf{d}[\mathbf{m}(\widetilde{\mathbf{m}})] = \mathbf{d}[exp(\widetilde{\mathbf{m}}) - \sigma_b]. \tag{B–3}$$

The variation of $\mathbf{d}$ with respect to $\widetilde{\mathbf{m}}$ can be found using the chain rule:

$$\delta_{\widetilde{\mathbf{m}}}\mathbf{d}(\widetilde{\mathbf{m}}) = \delta_{\widetilde{\mathbf{m}}}\mathbf{d}[\mathbf{m}(\widetilde{\mathbf{m}})] = \delta_{\mathbf{m}}\mathbf{d}(\mathbf{m})\delta_{\widetilde{\mathbf{m}}}\mathbf{m}. \tag{B–4}$$

Since

$$\delta_{\mathbf{m}}\mathbf{d}(\mathbf{m}) = \widehat{\mathbf{F}}(\mathbf{m}) = \widehat{\mathbf{F}}[exp(\widetilde{\mathbf{m}}) - \sigma_b], \tag{B–5}$$

where $\widehat{\mathbf{F}}$ is given by (37), (43) and (44), and

$$\delta_{\widetilde{\mathbf{m}}}\mathbf{m} = exp(\widetilde{\mathbf{m}})\delta\widetilde{\mathbf{m}}, \tag{B–6}$$

the result is

$$\delta_{\widetilde{\mathbf{m}}}\mathbf{d}(\widetilde{\mathbf{m}}) = \widehat{\mathbf{F}}^l(\widetilde{\mathbf{m}})\delta\widetilde{\mathbf{m}}, \tag{B–7}$$

where

$$\widehat{\mathbf{F}}^l(\widetilde{\mathbf{m}}) = \widehat{\mathbf{F}}[exp(\widetilde{\mathbf{m}}) - \sigma_b]exp(\widetilde{\mathbf{m}}) \tag{B–8}$$

is the Frechet derivative with respect to the logarithm of the total conductivity. Using this new space of model parameters, the models are realistic, and also the convergence of the iterative solver is usually faster. This coincides with Wannamaker (2000), who observed that the conversion into log resistivity decreases the nonlinearity of the forward operator for the two-dimensional magnetotelluric problem.

# Figure Captions

**Figure 1:** 3-D geoelectrical model of rectangular conductive prism embedded in a homogeneous half-space excited by a horizontal rectangular loop.

**Figure 2:** Behavior of the anomalous horizontal electric and vertical magnetic field components computed for the model in Figure 1 by solving the full integral equation (IE), quasi-analytical approximation (QA) and the diagonalized quasi-analytical approximation (DQA).

**Figure 3:** a) 3-D geoelectrical model of a tilted conductive dike embedded in a homogeneous half-space excited by a plane wave source (dike model). The discretization of the inverted area is also shown. The receivers are marked by dots right above the inverted area. b) Vertical cross-sections of the inverted area and the true dike model. The grid of the discretization of the inverted area is also displayed.

**Figure 4:** Vertical cross-sections of the predicted inverse model for the dike model after smooth DQA inversion of TM mode data. The full MT expression has been used as a forward operator introduced in Equation (24).

**Figure 5:** Vertical cross-sections of the predicted inverse model for the dike model after smooth DQA inversion of TM mode data. The linearized MT expression has been used as a forward operator introduced in Equation (27).

**Figure 6:** Vertical cross-sections of the predicted inverse model for the dike model after smooth and focusing Born inversions of joint TE and TM mode data.

**Figure 7:** a) Distribution of MT sounding sites in the Minamikayabe area. Stars denote the positions of MT sites. b) Three-dimensional sketch of the inverted

area and its discretization for the inversion of the Minamikayabe area data. The locations of the MT stations are marked by stars.

**Figure 8:** Sketch of a typical cross-section below the center of the inverted area of the Minamikayabe area, based on the 2-D interpretation of real MT data (redrawn from Takasugi et al., 1992).

**Figure 9:** Volume images of the predicted resistivity models after a) smooth and b) focusing DQA inversions of the Minamikayabe area data set.

**Figure 10:** Vertical cross-sections of the predicted inverse model obtained by a) smooth and b) focusing DQA inversions of the Minamikayabe area data set.

**Figure 11:** Pseudosections of the observed and predicted apparent resistivities and phases after the DQA inversion of the Minamikayabe area data set.

**Figure 12:** Block geology map of the Voisey's Bay area (top) and the corresponding magnetic map (bottom) (after Balch, 2000).

**Figure 13:** Maps of the observed TE mode apparent resistivities and phases at f = 95 Hz over the Voisey's Bay area. Dots mark the observation sites.

**Figure 14:** Three-dimensional sketch of the inverted area and its discretization for the inversion of the Voisey's Bay area data. The locations of the MT profiles are marked by thick black lines.

**Figure 15:** a) Vertical cross-sections and b) volume image of the predicted inverse resistivity model after a smooth DQA inversion of the Voisey's Bay area data set.

**Figure 16:** Volume image of the inversion results with resistivity below 25 ohm-m (top) and 50 ohm-m (bottom). The shallow anomalies are marked in black,

while the deep structures are painted in white.

**Figure 17:** Pseudosections of the observed and predicted apparent resistivities and phases after the DQA inversion of the Voisey's Bay area data set.

Table 1: CPU times of different inversions measured on a Sun Ultra Sparc 10 workstation

| The inverted area | | Data | | Inversion | |
|---|---|---|---|---|---|
| Discretization | Total No. of cells | No. of freqs. | Total No. of data | No. of iters. | CPU time, minutes |
| $15 \times 13 \times 9$ | 1755 | 4 | 1560 | 50 | 5 |
| $20 \times 5 \times 7$ | 700 | 11 | 1056 | 30 | 5 |
| $26 \times 26 \times 11$ | 7436 | 7 | 2366 | 40 | 10 |
| $56 \times 50 \times 12$ | 33600 | 5 | 2760 | 30 | 14 |

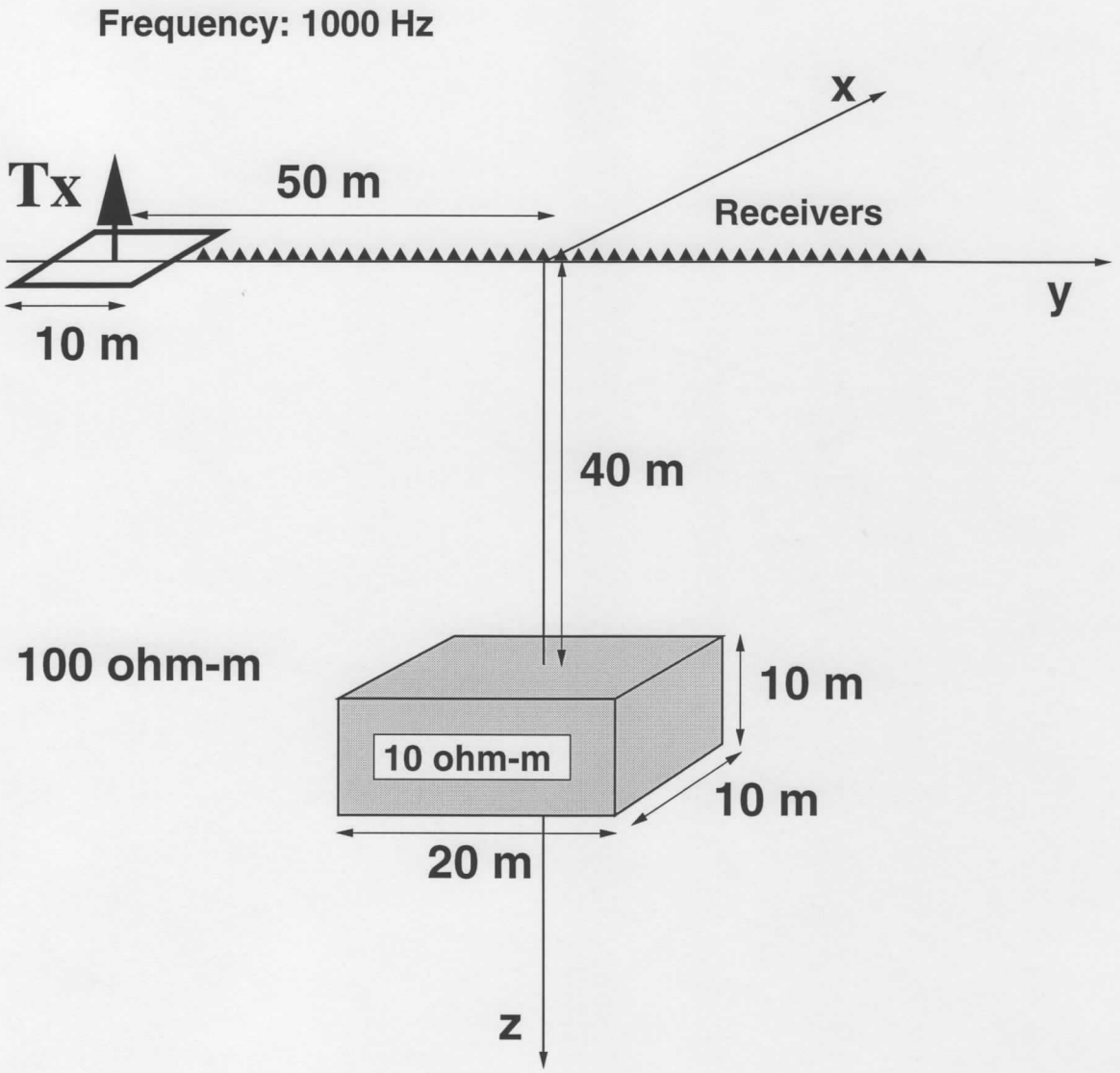


Figure 1: 3-D geoelectrical model of rectangular conductive prism embedded in a homogeneous half-space excited by a horizontal rectangular loop.

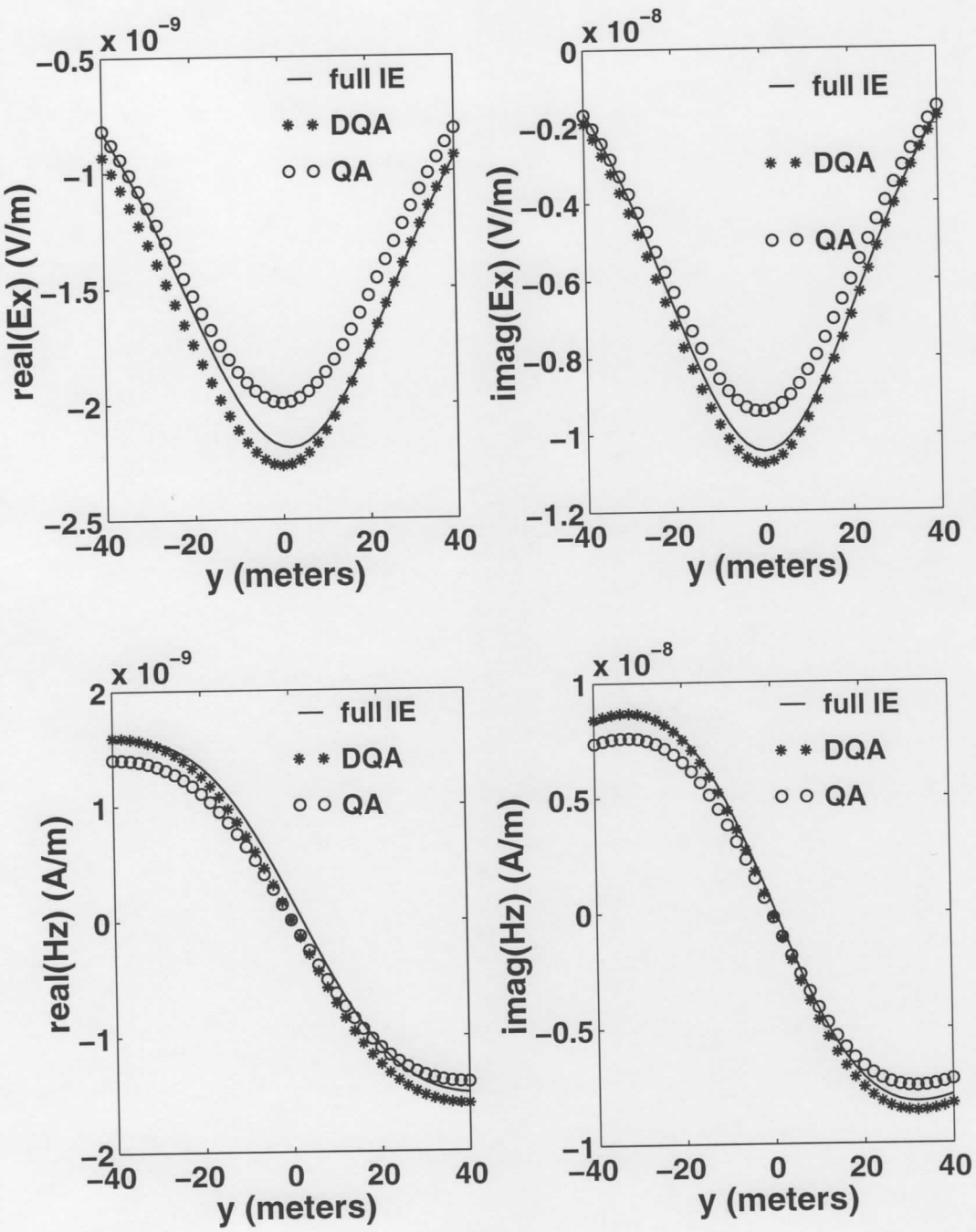


Figure 2: Behavior of the anomalous horizontal electric and vertical magnetic field components computed for the model in Figure 1 by solving the full integral equation (IE), quasi-analytical approximation (QA) and the diagonalized quasi-analytical approximation (DQA).

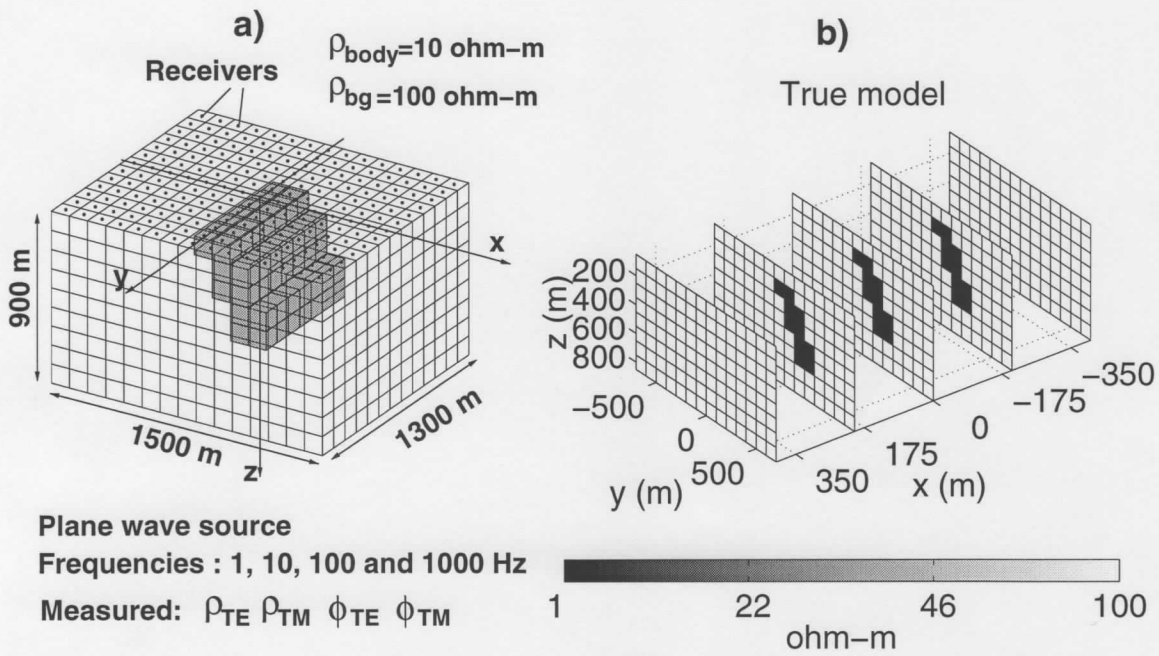


Figure 3: a) 3-D geoelectrical model of a tilted conductive dike embedded in a homogeneous half-space excited by a plane wave source (dike model). The discretization of the inverted area is also shown. The receivers are marked by dots right above the inverted area. b) Vertical cross-sections of the inverted area and the true dike model. The grid of the discretization of the inverted area is also displayed.

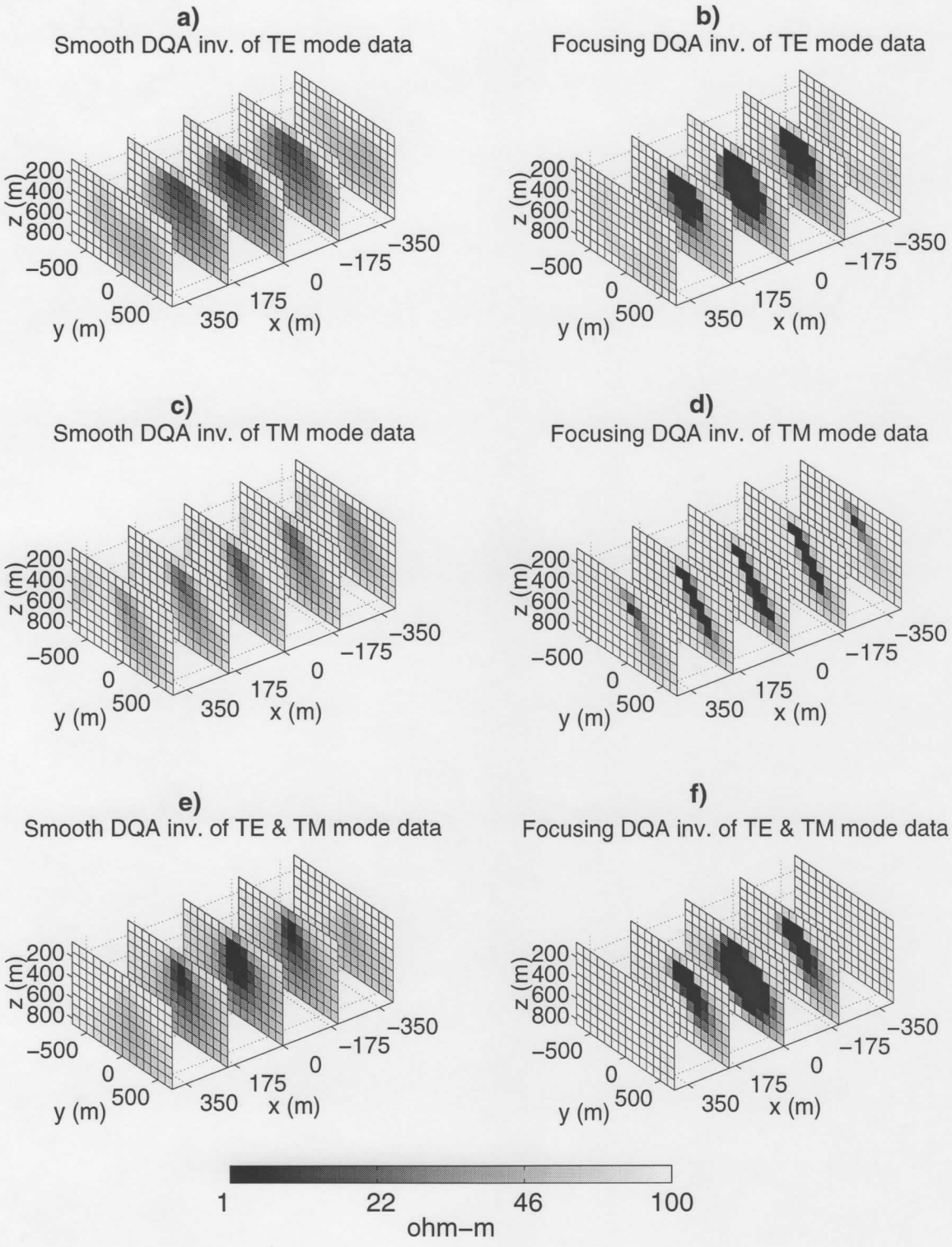


Figure 4: Vertical cross-sections of the predicted inverse model for the dike model after smooth DQA inversion of TM mode data. The full MT expression has been used as a forward operator introduced in Equation (24).

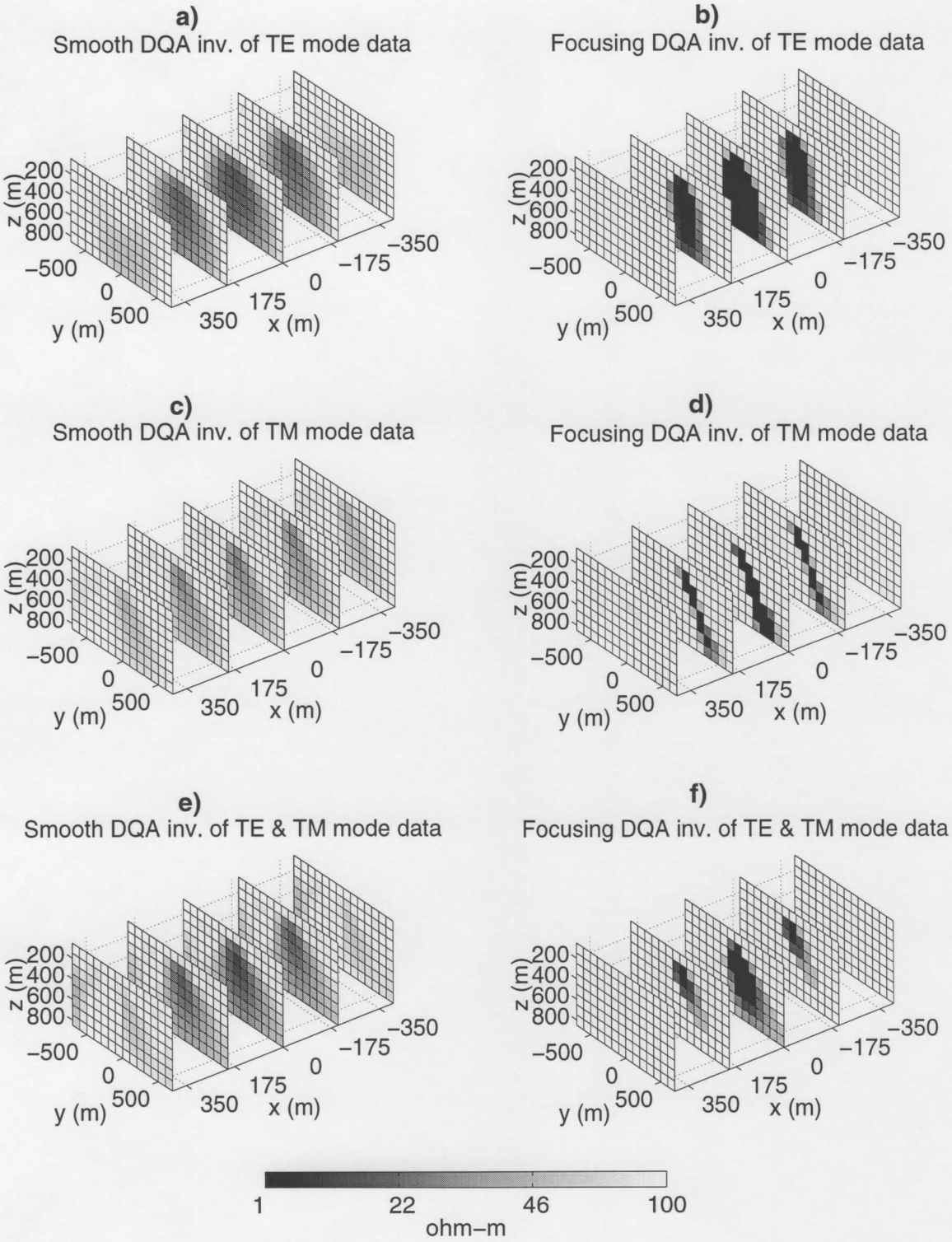


Figure 5: Vertical cross-sections of the predicted inverse model for the dike model after smooth DQA inversion of TM mode data. The linearized MT expression has been used as a forward operator introduced in Equation (27).

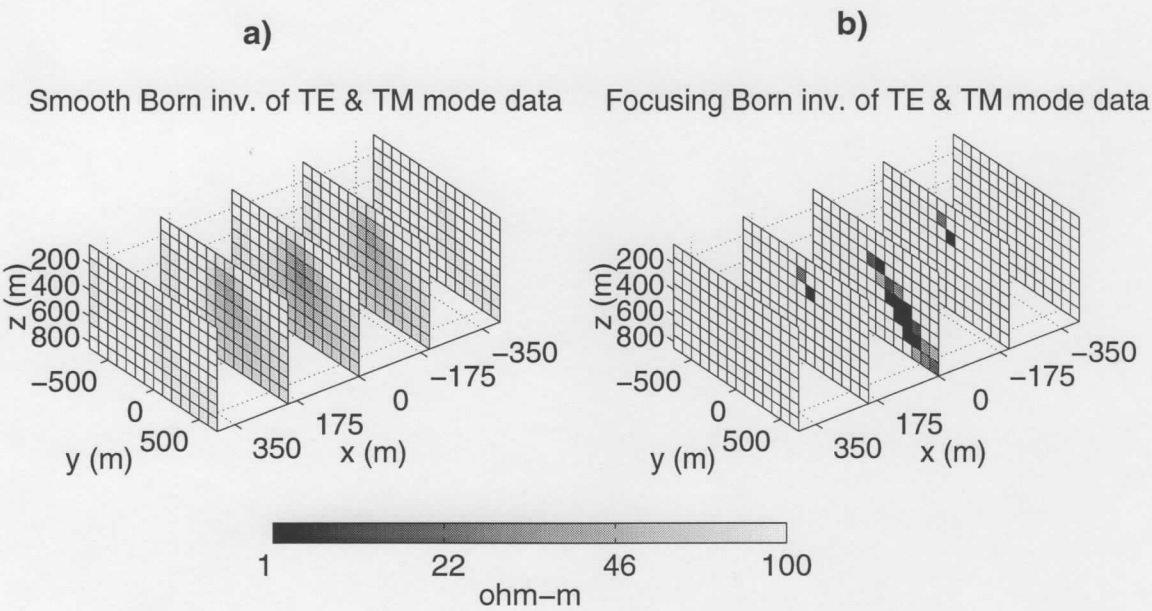


Figure 6: Vertical cross-sections of the predicted inverse model for the dike model after smooth and focusing Born inversions of joint TE and TM mode data.

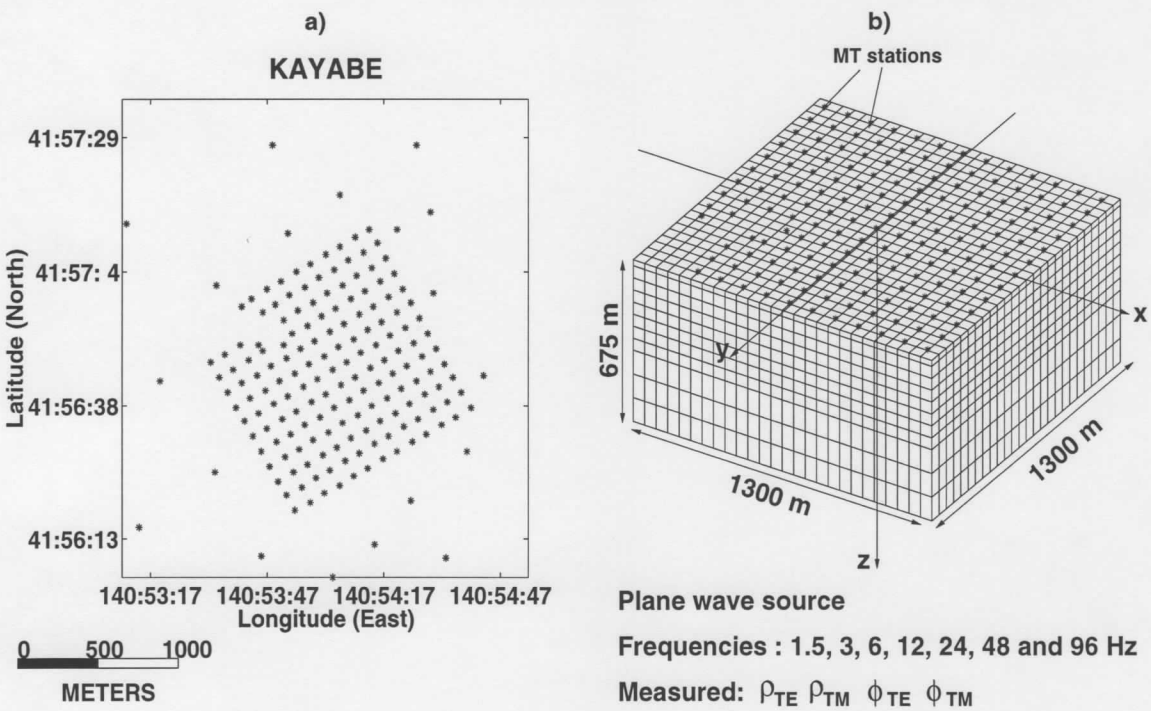


Figure 7: a) Distribution of MT sounding sites in the Minamikayabe area. Stars denote the positions of MT sites. b) Three-dimensional sketch of the inverted area and its discretization for the inversion of the Minamikayabe area data. The locations of the MT stations are marked by stars.

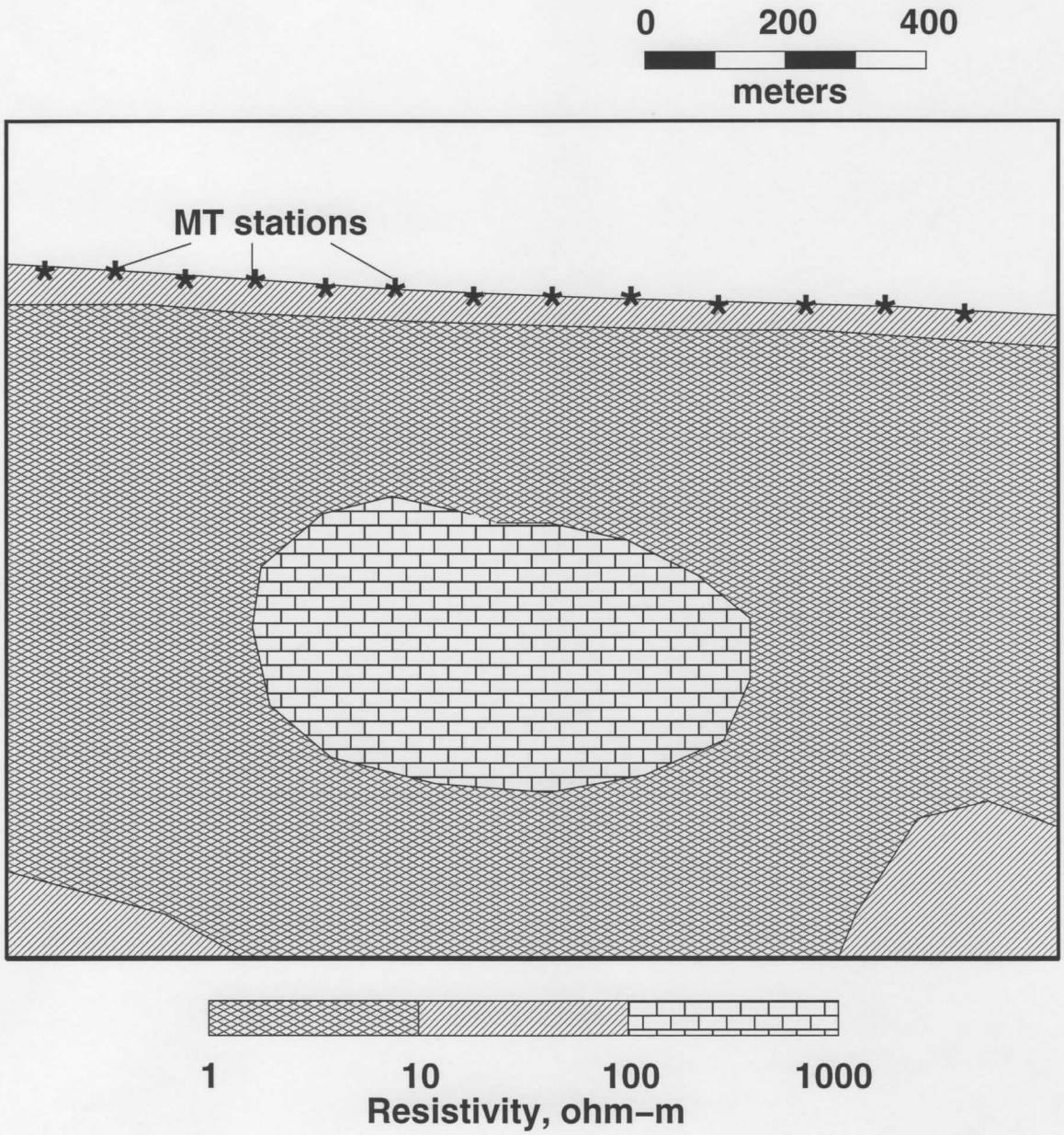


Figure 8: Sketch of a typical cross-section below the center of the inverted area of the Minamikayabe area, based on the 2-D interpretation of real MT data (redrawn from Takasugi et al., 1992).

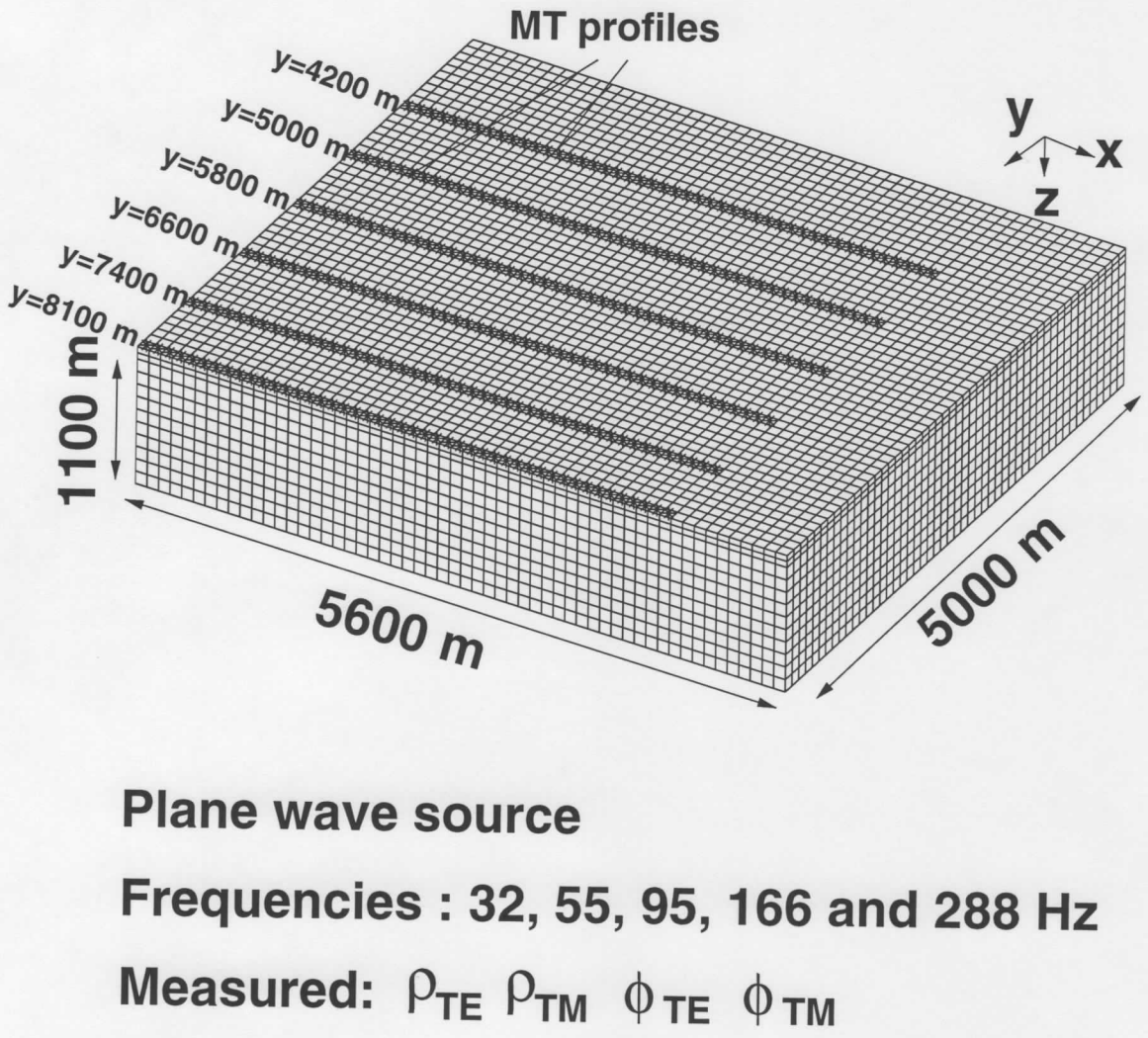


Figure 14: Three-dimensional sketch of the inverted area and its discretization for the inversion of the Voisey's Bay area data. The locations of the MT profiles are marked by thick black lines.

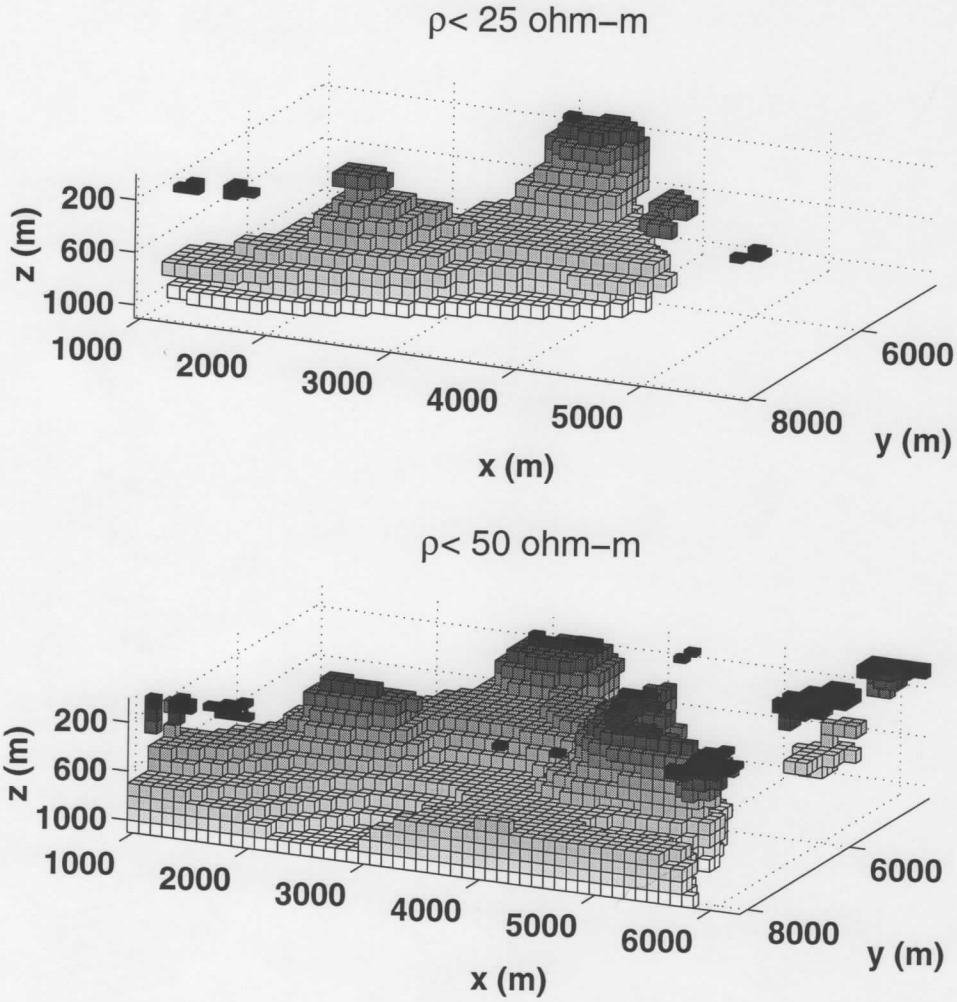


Figure 16: Volume image of the inversion results with resistivity below 25 ohm-m (top) and 50 ohm-m (bottom). The shallow anomalies are marked in black, while the deep structures are painted in white.